J Neuropathol Exp Neurol
Vol. 77, No. 3, March 2018, pp. 246–259
doi: 10.1093/jnen/nlx120

ORIGINAL ARTICLE

Tau Oligomer Pathology in Nucleus Basalis Neurons During the Progression of Alzheimer Disease

Chelsea T. Tiernan, PhD, Elliott J. Mufson, PhD, Nicholas M. Kanaan, PhD, and Scott E. Counts, PhD

Abstract

Although tau is the primary constituent of neurofibrillary tangles (NFTs), evidence suggests that its toxic moiety is oligomeric in Alzheimer disease (AD). In this regard, tau oligomers correlate more strongly with neuronal loss than NFTs and exhibit neurotoxicity in preclinical AD models. Here, we investigated the spatiotemporal progression of oligomeric tau accumulation within the highly vulnerable cholinergic neurons of the nucleus basalis of Meynert (nbM) in AD. Tissue from subjects who died with a clinical diagnosis of no cognitive impairment, mild cognitive impairment, or AD was immunostained with the tau oligomeric complex 1 (TOC1) antibody, a marker of tau oligomers, and $p75^{NTR}$, a cholinergic cell marker. Stereological estimates revealed a significant increase in the number of TOC1 nbM immunopositive (+) neurons with a concomitant decrease in $p75^{NTR}$+ nbM neurons during the transition from mild cognitive impairment to AD. Immunofluorescence identified TOC1+ neurons that colocalized with the pretangle tau marker phospho-Ser422, which persisted into late stage NFTs immunoreactive for MN423. Analysis of the nbM subfields revealed a topographical caudal to rostral gradient of TOC1+ neurons during disease progression. Taken together, these data suggest that toxic tau oligomers accumulate caudorostrally in selectively vulnerable nbM neurons during the onset of AD.

Key Words: Alzheimer disease, Basal forebrain, Mild cognitive impairment, Nucleus basalis of Meynert, Oligomeric, Phosphorylation, Tauopathy.

INTRODUCTION

Cholinergic basal forebrain (CBF) neurons residing within the nucleus basalis of Meynert (nbM; Ch4) form a continuum of subfields extending from the anterior subfield at the level of the crossing of the anterior commissure (Ch4a), which is further divided into anterior-medial (Ch4am) and anterior-lateral (Ch4al) sectors, to the intermediate subfield at the recession of this commissure (Ch4i), to the posterior subfield (Ch4p) at the level of the lateral geniculate nucleus (1, 2). These neurons provide the major source of acetylcholine throughout the cortical mantle and amygdala (1, 2). Degeneration of Ch4 neurons correlates with cognitive impairment, dementia severity, and disease duration in Alzheimer disease (AD) (3–10). Recent studies from our group suggest that pathological events underlying the formation of neurofibrillary tangles (NFTs) containing pathological tau within CBF neurons occur early during the progression of AD (11, 12). These cellular events involve the appearance of discrete tau neoepitopes, which undergo a pathological sequence of posttranslational modifications precipitating NFT formation (11, 12). CBF NFTs are found in close association with tau-positive neuropil threads during the early stages of AD progression (13). Furthermore, evidence suggests that CBF neuronal subfield degeneration and cell loss follow a caudal to rostral topographical progression (9, 10, 14–16). However, the spatiotemporal distribution of tau pathologies, such as aberrantly phosphorylated, truncated, or oligomeric tau, in the basocortical cholinergic projection subfields has yet to be characterized during the clinical progression of AD.

Although NFTs are implicated in mediating cognitive decline in AD (17–20), accumulating evidence suggests that prefibrillar oligomers are likely the more neurotoxic species of tau (1, 2, 21–25). For instance, reducing tau overexpression decreases neuronal cell loss even though filamentous inclusions continue to form (3–10, 26), and multimeric tau species correlate with spatial memory deficits in the rTg4510 transgenic tauopathy mouse (11, 12, 21). Moreover, oligomeric tau disrupts CA3-CA1 long-term potentiation in mouse hippocampal slice preparations, suggesting a role in mediating synaptic dysfunction in memory circuits (27). In human frontal cortex, levels of granular tau oligomers are elevated, even in early Braak stages I–II (11, 12, 23, 24, 28) when NFTs are not apparent in this region (13, 29). However, the extent of the accumulation of tau oligomeric species in the cholinergic nbM neurons during the progression of AD has yet to be evaluated.

From the Department of Translational Science and Molecular Medicine (CTT, NMK, SEC); Department of Family Medicine, Michigan State University, Grand Rapids, Michigan (SEC); Mercy Health Saint Mary's Hospital, Hauenstein Neurosciences Center, Grand Rapids (NMK, SEC); Michigan Alzheimer's Disease Core Center, Ann Arbor, Michigan (SEC); and Department of Neurobiology, Barrow Neurological Institute, Phoenix, Arizona (EJM)

Send correspondence to: Scott E. Counts, PhD, Department of Translational Science and Molecular Medicine, Michigan State University, 400 Monroe Ave. NW, Grand Rapids, MI 49503. E-mail: scott.counts@hc.msu.edu

Nicholas M. Kanaan and Scott E. Counts contributed equally to this work.

This work was supported by NIH grants AG014449, AG053581, AG053760, NS082730, AG044372 as well as the Saint Mary's Foundation, Miles for Memories of Battle Creek, MI, Barrow Neurological Institute Barrow and Beyond, and a grant for the Arizona ADC.

The authors have no duality or conflicts of interest to declare.

Supplementary Data can be found at http://www.jnen.oxfordjournals.org.

In this study, we used a monoclonal antibody that selectively recognizes oligomeric tau, tau oligomeric complex 1 (TOC1) (9, 10, 14–16, 24), combined with an antibody against the low-affinity nerve growth factor (NGF) receptor $p75^{NTR}$, an excellent marker for cholinergic nbM neurons (10, 17–20), to characterize the spatiotemporal accumulation of tau multimers within perikarya of the CBF subfields in postmortem tissue obtained from participants in the Rush Religious Orders Study (RROS) who died with an antemortem clinical diagnosis of no cognitive impairment (NCI), mild cognitive impairment (MCI), or AD. We also performed confocal microscopy to assess the colocalization of TOC1 immunoreactivity with markers for early pretangle and mature tangle pathology. Quantitation of single-labeled $p75^{NTR}$ immunopositive (+), TOC1+, and dual-labeled $p75^{NTR}$+/TOC1+ neurons within the nbM subfields was estimated by unbiased stereology and correlated with clinical test scores and neuropathologic diagnostic criteria during disease progression. Our data provide evidence that tau oligomers associate with pretangle pathology within cholinergic nbM neurons and appear early in the NCI-MCI-AD continuum. Moreover, tau oligomer accumulation follows a caudorostral gradient throughout the Ch4 subgroups that mirrors the topographical pattern of Ch4 neuronal selective vulnerability and cell loss during disease progression. These data suggest that tau oligomer formation is an early event that contributes to the spatiotemporal pattern of CBF neuron dysfunction during the onset of AD.

MATERIALS AND METHODS

Subjects

Individuals examined were all participants in the RROS, a longitudinal clinical-pathological study of aging and AD of elderly retired Catholic nuns, priests, and brothers (30–33). Rush University Medical Center and Michigan State University Institutional Review Boards approved the study. The present investigation is based on 12 individuals meeting clinical criteria for NCI, 9 for MCI, and 12 for mild AD (Table 1). All subjects came to autopsy with no coexisting clinical conditions contributing to cognitive impairment as judged by the examining neurologist and were not receiving anticholinesterase drug therapy.

Clinical Evaluation

Details of the RROS clinical evaluation and diagnostic criteria are published (30, 33–36). Briefly, a team of investigators performed an annual clinical evaluation, including a medical history and interview for common problems of elderly persons, a complete neurological examination, and cognitive performance testing with the Mini-Mental State Exam (MMSE) and 17 additional neuropsychological tests referable to 5 cognitive domains: orientation, attention, memory, language, and perception (37, 38). A global cognitive score (GCS), consisting of a composite *z*-score calculated from this test battery also was determined for each participant. A board-certified neurologist with expertise in the evaluation of the elderly, and blinded to age, sex, race/ethnicity, and clinical data other than occupation, education, and information about sensory or motor deficits, used these results to summarize impairments in each of the 5 cognitive domains. The diagnosis of dementia or AD met recommendations by the joint working group of the National Institute of Neurologic and Communicative Disorders and Stroke/AD and Related Disorders Association (NINCDS/ADRDA) (39). The MCI population was defined as subjects who exhibited cognitive impairment on neuropsychological testing but did not meet the criteria for AD or dementia, criteria consistent with those used by others in the field (40–43). Cases with complicating conditions, such as stroke, Parkinson disease, Lewy body dementia, hippocampal sclerosis, and major depressive disorder, were excluded.

Brain Tissue Preparation and Pathological Evaluation

Brains were removed from the calvarium at autopsy (mean postmortem interval, 4.8 hours; range, 1.0–8.6 hours; Table 1) and processed as previously described (30, 33, 36). Briefly, 1 hemisphere of each brain was cut on a brain-slice apparatus into 1-cm-thick slabs, immersion fixed in 4% paraformaldehyde in 0.1 M phosphate buffer, pH 7.2, at 4°C for 48 hours, and cryoprotected in 10% glycerol plus 2% dimethyl sulfoxide (DMSO) in 0.1 M phosphate buffer at 4°C for 2–7 days, followed by immersion in a solution of 20% glycerol plus 2% DMSO. Brain slabs containing the CBF were cut into 18 series (720-μm interval) of adjacent 40-μm-thick sections on a freezing, sliding stage microtome, and stored in cryoprotectant solution until processed. Select regions from the opposite hemisphere were paraffin-embedded, cut at 8 μm, and stained with hematoxylin and eosin, modified Bielschowsky, thioflavin-S, and AT8-tau and ubiquitin antibodies for neuropathological diagnosis (44).

A board-certified neuropathologist evaluated all cases blinded to clinical diagnosis. Designations of "normal" (with respect to AD or other dementing processes), "possible AD," "probable AD," or "definite AD" were based on semiquantitative estimation of neuritic plaque density, an age-related plaque score, and presence or absence of dementia as established by the Consortium to Establish a Registry for Alzheimer's Disease (CERAD) (45). Braak scores based on the staging of NFT pathology were established for each case (46). Cases received a Reagan likelihood-of-AD diagnosis based on plaque and tangle pathology (47). The recent algorism for the diagnosis of AD (48) is currently being applied to all RROS cases.

Antibodies

The mouse monoclonal antibody TOC1 was raised against photochemically cross-linked tau dimers (24). The TOC1 epitope (amino acids 209–224) is conformation dependent and reacts with tau dimers and oligomeric assemblies (49). The specificity of TOC1 for tau oligomers was previously confirmed by immunoblotting and immunolabeled electron microscopy (24, 49).

A mouse monoclonal antibody generated against the low-affinity NGF receptor ($p75^{NTR}$) was created from A875 melanoma cells as the immunogen, affinity purified, and

TABLE 1. Demographic, Clinical, and Neuropathological Characteristics by Diagnosis

	Clinical Diagnosis				
	NCI (n = 12)	MCI (n = 9)	AD (n = 12)	Total (n = 33)	Comparison by Diagnosis Group (p Value)
Age at death (years)					
Mean ± SD	85.2 ± 4.4	87.5 ± 4.9	88.2 ± 5.2	86.9 ± 4.9	0.3
(range)	(78–93)	(79–94)	(76–95)	(76–95)	
No. (%) Males	3 (25)	4 (44)	2 (25)	9 (30)	0.4*
Years of education					
Mean ± SD	17.3 ± 4.2	16.9 ± 3.4	18.9 ± 3.4	17.8 ± 3.7	0.4
(range)	(10–25)	(10–20)	(14–26)	(10–26)	
Postmortem interval (hours)					
Mean ± SD	4.8 ± 2.0	5.2 ± 2.0	4.5 ± 1.9	4.8 ± 1.9	0.7
(range)	(1.0–8.1)	(2.0–8.6)	(1.5–8.1)	(1.0–8.6)	
No. (%) with ApoE±4 allele	0 (0)	3 (33)	6 (50)	9 (27)	0.02*
MMSE					
Mean ± SD	28.3 ± 1.7	27.4 ± 2.4	18.7 ± 8.7	24.4 ± 6.8	0.0001†
(range)	(26–30)	(23–30)	(2–28)	(2–30)	
Global cognitive score					
Mean ± SD	−0.1 ± 0.2	−0.5 ± 0.3	−1.7 ± 0.8	−0.8 ± 0.9	0.0001†
(range)	(−0.4, 0.3)	(−0.9, 0.0)	(−3.7, −0.9)	(−3.7, 0.3)	
Braak scores					
I–II	4	1	1	6	
III–IV	7	6	5	18	0.08
V–VI	1	2	6	9	
NIA Reagan diagnosis (likelihood of AD)					
No AD	0	0	0	0	
Low	8	4	1	13	0.006‡
Intermediate	4	3	7	14	
High	0	2	4	6	
CERAD diagnosis (likelihood of AD)					
No AD	3	3	0	6	
Low	3	1	0	4	0.05‡
Intermediate	6	3	8	17	
High	0	2	4	6	

AD, Alzheimer disease; MCI, mild cognitive impairment; MMSE, mini-mental status exam; NCI, no cognitive impairment; SD, standard deviation.
*Chi-square test.
†Pairwise comparisons with Tukey's correction showed no difference between NCI and MCI, but both were significantly different from AD.
‡Pairwise comparisons with Tukey's correction showed a significant difference between NCI and AD only.

characterized by immunohistochemistry and flow cytometry as described by the manufacturer (Thermo Scientific, OSM00019A). Previous work demonstrated the specificity of $p75^{NTR}$ for human cholinergic nbM neurons (10, 50, 51).

Two additional antibodies were used to characterize the appearance of tau oligomer pathology within the temporal evolution of NFTs within CBF neurons. A rabbit monoclonal anti-Tau pS422 antibody was used to identify early stage (pre-tangle) tau pathology (12, 52–54). The pS422 antibody is an affinity-purified antibody that was raised against a synthetic peptide containing phosphoserine 422 (S422) of human tau, and characterized by Western blotting as described by the manufacturer (Abcam, ab79415). The mouse monoclonal MN423 antibody was used to identify late-stage tau pathology (55–7). MN423 was raised against an enriched preparation of paired helical filaments and detects tau truncated at glutamic acid 391 (E391), a modification that occurs during the later stages of tangle evolution (57–59).

Immunohistochemistry

A series of sections containing Ch4 subregions was processed for TOC1 and $p75^{NTR}$ using a double-labeled immunohistochemical procedure (12). Tissue was rinsed 6 × 10 minutes with 0.1 M tris buffer saline ([TBS]; pH 7.4) containing 0.05% Triton X-100 (TxTBS) before each step of the staining protocol and all steps were performed at room temperature, unless otherwise specified. Endogenous peroxidase activity was quenched by incubating the tissue in 3% H_2O_2 for 1 hour. Nonspecific binding was inhibited by incubating for 1 hour in blocking buffer containing 10% normal goat serum (NGS)/2% bovine serum albumin (BSA)/TxTBS. Immediately

following blocking, tissue was incubated with the first primary antibody (TOC1; 1:2,000) in dilution buffer (2% NGS/TxTBS) at 4°C overnight. The following day tissue was incubated with biotinylated goat antimouse IgM secondary antibody (Vector Laboratories, BA-2020) diluted 1:500 in dilution buffer for 2 hours, before incubation in avidin-biotin complex (Vector Laboratories, PK-6100) made according to manufacturer's instructions. Tissue was developed in 0.25% ammonium nickel (II) sulfate hexahydrate (Sigma, A1827), 0.05% 3′,3′-diaminobenzidine, and 0.003% H_2O_2 resulting in a black reaction product.

Subsequently, tissue was incubated in an avidin/biotin blocking kit (Vector Laboratories, SP-2001) following the manufacturer's recommendations. Any remaining peroxidase activity from the first reaction was quenched with 3% H_2O_2 for 30 minutes. Tissue was blocked for 1 hour in blocking buffer, and then immediately incubated at 4°C overnight with the second primary antibody ($p75^{NTR}$; 1:120,000) in dilution buffer. The next day, the tissue was incubated with biotinylated goat antimouse IgG (Vector Laboratories, BA-9200) diluted 1:500 in dilution buffer for 2 hours, before incubation in avidin-biotin complex solution as described above. Tissue was developed in 0.05% 3′,3′-diaminobenzidine and 0.003% H_2O_2 to produce a brown reaction product. After development, tissue was mounted on microscope slides (VWR, 16004-406), air-dried for no more than 6 hours, dehydrated is a series of graded ethanols (70%, 90%, 95%, and 100%), cleared in xylenes, and coverslipped using CytoSeal 60 (Thermo Scientific, 8310).

Appropriate immunohistochemistry controls were performed to rule out cross-reactivity and nonspecific staining. Omission of both primary antibodies resulted in no detectable immunostaining. Omission of either TOC1 or $p75^{NTR}$ primary antibody detected only the specific epitope of the respective primary antibody, and ensured that quenching and blocking steps were effective (Supplementary Data Fig. S1).

Immunofluorescence

To evaluate the appearance of TOC1 immunoreactive (+) neurons in the temporal sequence of tangle maturation, additional forebrain sections from 6 NCI, 6 MCI, and 6 AD cases, selected randomly from the above cases, were processed for immunofluorescence. Tissue was rinsed 6 × 10 minutes with TxTBS before each step of the staining protocol and all steps were performed at room temperature, unless otherwise specified. Tissue was blocked for 1 hour in 10% NGS/2% BSA/TxTBS, and then incubated at 4°C overnight with all 3 primary antibodies diluted in 2% NGS/TxTBS (TOC1, 1: 2,000; pS422, 1: 2,500; MN423, 1:500). The following day, the tissue was incubated with secondary antibodies for 2 hours. pS422 was labeled with Alexa Fluor 405 goat antirabbit (Invitrogen, A-31556), TOC1 with Alexa Fluor goat antimouse IgM 488 (Invitrogen, A-21042), and MN423 with Alexa Fluor goat antimouse IgG2b 568 (Invitrogen, A-21144). Tissue was rinsed, mounted on adhesive microscope slides, and dried overnight. Autofluorescence was blocked using Sudan black (11, 60–62), and slides were coverslipped using hardset Vectashield mounting media (Vector Laboratories H-1400).

Immunofluorescence controls were performed to rule out cross-reactivity and nonspecific staining. The following sets of controls were performed: 1) omission of all 3 primary antibodies, and 2) omission of TOC1, pS422, or MN423 primary antibody individually. All controls produced the expected results (Supplementary Data Fig. S2).

TABLE 2. Coefficients of Error for Quantification of Each Marker

Stereological Count	Range	Mean ± SEM
$p75^{NTR}$+	0.05–0.1	0.07 ± 0.003
$p75^{NTR}$/TOC1+	0.05–1.0	0.21 ± 0.04
TOC1+	0.07–1.0	0.27 ± 0.04

$p75^{NTR}$, low-affinity neurotrophin receptor; TOC1, tau oligomer complex 1; SEM, standard error of mean.

Stereological Quantification of Neurons

Quantitative estimates of the number of $p75^{NTR}$+, $p75^{NTR}$+/TOC1+, and TOC1+ neurons within Ch4 subfields were performed using the optical fractionator cell counting protocol (31, 60, 63–65). The region of interest, containing the Ch4 neurons, extends from the crossing of the anterior commissure to the level of the lateral geniculate nucleus (1, 66). The optical fractionator methods allow for the unbiased analysis of a well-defined portion of a structure independent of its size, shape, orientation, or tissue shrinkage (64, 67, 68).

The stereology system consisted of a Nikon Eclipse 80i microscope (Nikon Instruments) hard-coupled to an MAC5000 computer-controlled x-y-z motorized stage (Ludl Electronic Products, Hawthorne, NY), a Microfire A/R video system (Optronics, Goleta, CA), and a computer equipped with StereoInvestigator v9.0 software (MBF Bioscience, Williston, VT). Neuronal cell counts were performed on a 1:18 series of sections that yielded an average of 16 serial sections per case. The CBF region was outlined at low magnification using a 2× objective and approximately 200–400 immunoreactive neurons were counted at 60× magnification with a counting frame of 10 mm^2. The percentage of area counted was adjusted for each cell type to achieve the most accurate estimate possible, but the methods used for each case were uniform throughout all sections. For the $p75^{NTR}$+ neurons, 5% of the outlined CBF area was counted for all cases. TOC1+ and $p75^{NTR}$+/TOC1+ neurons were relatively sparse, and therefore were counted at 100% of the area. The average section thickness was 13.2 μm and a guard zone of 1 μm was applied to the top and bottom of each section. Coefficients of error (CE) were calculated using the Gundersen method to estimate the accuracy of the optical fractionator probe (64, 69, 70). The mean and range of the CE values for each cell phenotype counted are listed in Table 2. The stereologist performing the quantitative analysis was blinded to age, gender, and clinical and pathological classification of each subject analyzed.

To evaluate the spatial progression of TOC1+ pathology in the cholinergic subgroups of the nbM, serial sections from each case included in the stereological quantification were separated into anterior, intermediate, and posterior subfields, based on previously established anatomical boundaries (1, 2, 10, 66). Briefly, Ch4a begins as scattered cells just caudal to the olfactory tubercle, reaching its greatest extent rostrocaudally at the crossing of the anterior commissure. Cells of Ch4i were identified by the presence of the ansa peducularis, and cell density is highest at this level. The posterior subfield of the CBF was defined by the presence of the cerebral peduncle, and lower cellular density as compared to the intermediate subfield. The estimated number of cells in each subfield was analyzed by Ch4 subregion for each cell phenotype (i.e. $p75^{NTR}$+, TOC1+, or $p75^{NTR}$+/TOC1+) and the data are reported as the percentage of the total estimated cell count per subfield and the ratio of TOC1+ neurons counted ($p75^{NTR}$+/TOC1+ and TOC1+) to $p75^{NTR}$+ neurons counted ($p75^{NTR}$+ and $p75^{NTR}$+/TOC1+).

TOC1 Colocalization

One section representative of TOC1+ pathology in the intermediate (Ch4i) subfield was selected from 6 NCI, 6 MCI, and 6 AD cases and triple-labeled with TOC1, pS422, an MN423, as described above. Large multipanel images encompassing the entire Ch4i subfield were collected at 10× magnification on a Nikon A1+ laser scanning confocal microscope system equipped with solid state lasers (405, 488, 561) and Nikon Elements AR software. TOC1+ neurons within the CBF were identified, and cells were counted according to one of the following phenotypes: 1) TOC1+, 2) TOC1+/pS422+, 3) TOC1+/MN423+, or 4) TOC1+/pS422+/MN423+. Counts are displayed as the percentage of total TOC1+ neurons per section that were either single-, double-, or triple-labeled.

Statistics

Demographic, clinical, and neuropathological characteristics were analyzed by either Fisher exact test or 1-way analysis of variance with Tukey's correction for post hoc comparison. Neuron counts were compared across clinical diagnostic groups with 1-way analysis of variance, and assessed for association with demographic, clinical, and neuropathological variables by Pearson correlation (71, 72). Data were transformed by natural logarithm as needed. All applicable tests were 2-tailed, and statistical significance was set at $p \leq 0.05$. GraphPad Prism 6 software (GraphPad Software, Inc., La Jolla, CA) was used for all statistical tests.

RESULTS

Clinical and Pathological Characteristics

Demographic, clinical, and neuropathological characteristics of the 33 subjects (12 NCI, 9 MCI, and 12 mild/moderate AD) are summarized in Table 1. There were no significant differences in age, gender balance, years of education, or postmortem interval. Subjects with AD had significantly lower MMSE scores ($F_{[2,\ 30]}=12.02$, $p=0.0001$) and GCS ($F_{[2,\ 30]}=28.19$, $p<0.0001$) compared to the NCI and MCI groups. NCI cases met the criteria for Braak stages I/II (33%), III/IV (58%), and IV/V (8%), MCI cases for Braak stages I/II (11%), III/IV (67%), and IV/V (22%), and AD cases for Braak stages I/II (8%), III/IV (42%), and IV/V (50%). Distribution of Braak scores was not significantly different across the diagnostic groups; however, NIA Reagan diagnosis ($F_{[2,\ 30]}=6.065$, $p=0.0006$) and CERAD score ($F_{[2,\ 30]}=5.076$, $p=0.013$) significantly differentiated NCI from AD subjects. In several cases, neuropathological scores were discordant with the clinical diagnosis (Table 1). For example, 1 NCI subject was Braak stage V and 3 were Braak stage IV. In addition, 33% and 50% of NCI subjects, respectively, had an intermediate likelihood of AD as evaluated by NIA Reagan diagnosis and CERAD. Similar findings were reported by us and others (73–75), suggesting that either these individuals tolerate NFT load in the medial temporal lobe without cognitive impairment, or were preclinical AD cases.

Morphology and Quantification of $p75^{NTR}$+, $p75^{NTR}$+/TOC1+, and TOC1+ Neurons

Sections immunostained for $p75^{NTR}$+ revealed a continuum of magnocellular neurons extending from Ch4am to Ch4al and to Ch4i subfields of the nbM in all cases, as previously described (10, 12, 76). By contrast, not all cases contained the Ch4p subfield (see below). Interstitial $p75^{NTR}$+ neurons were scattered throughout the internal capsule, medullary laminae of the globus pallidus, ansa peduncularis, and ansa lenticularis.

Neuronal cytoplasm and processes immunolabeled with $p75^{NTR}$ appeared brown (Fig. 1G) and TOC1 immunoreactivity displayed a black reaction product (Fig. 1J). Initially, TOC1 pathology appeared as faint black reactivity scattered within the cytoplasm (Fig. 1H). As pathology progressed, TOC1 immunoreactivity filled the entire neuronal cytoplasm before extending into the proximal processes (Fig. 1I). Single-labeled TOC1+ neurons often appeared shrunken and globose in appearance (Fig. 1J; black arrow). Flame-shaped NFTs were observed less frequently.

Quantification of $p75^{NTR}$+, $p75^{NTR}$+/TOC1+, and TOC1+ neurons was performed on all 33 subjects across the 3 clinical groups (Table 3). The number of $p75^{NTR}$+ nbM neurons decreased significantly in AD compared to NCI (Fig. 2A; $F_{[2,\ 30]}=3.407$, $p=0.046$). The number of $p75^{NTR}$+/TOC1+ nbM neurons progressively increased throughout the transition from NCI to MCI to AD (Fig. 2B). The number of single-labeled TOC1+ nbM neurons remained low in NCI and MCI, increasing only in AD subjects (Fig. 2C); however, group comparisons did not reach statistical significance (Table 3). Notably, a subanalysis of $p75^{NTR}$+, $p75^{NTR}$+/TOC1+, and TOC1+ nbM neurons in NCI cases classified as Braak stages I–II ($n=4$) compared to those with a high Braak score (Braak stages III–V, $n=8$) revealed no significant differences in $p75^{NTR}$+ neuron number ($p=0.9$ via Welch's t-test) or TOC1+ neuron number ($p=0.07$) between the 2 groups. However, we found a significant increase in the number of $p75^{NTR}$+/TOC1+ dual-labeled neurons in the NCI-high pathology group compared to the NCI-low pathology group

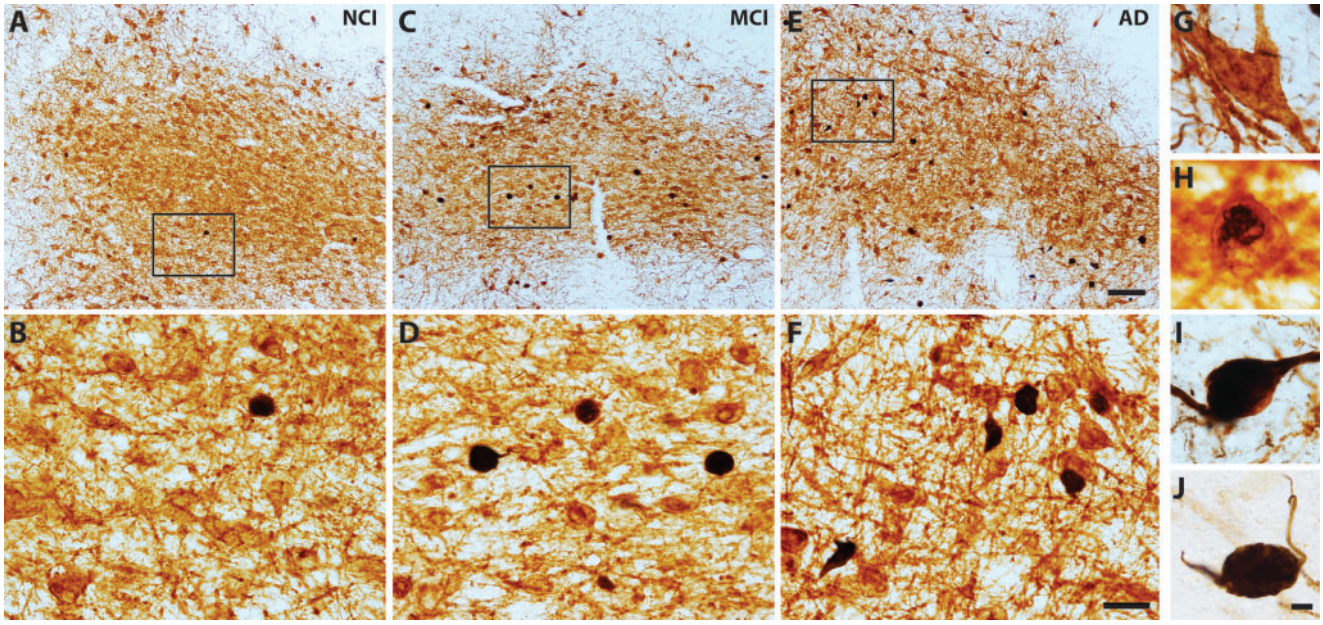

FIGURE 1. Dual p75^{NTR}/TOC1-immunoreactive neurons. Tissue sections containing the nbM immunostained for p75^{NTR} (**G**; brown) and TOC1 (**J**; black) show a modest increase in the number of p75^{NTR}+/TOC1+ neurons during the progression from NCI **(A, B)**, to MCI **(C, D)** and AD **(E, F)**. Panels **(B, D, F)** are high-magnification images of boxed area in **(A, C, E)**, respectively. TOC1+ pathology initially appeared within the cytoplasm **(G, H)** before forming a globose tangle and extending into proximal processes **(I)**. Scale bars: **E** = 200 μm, and also applies to **A** and **C**; **F** = 50 μm, and also applies to **B** and **D**; **J** = 10 μm, and also applies to **G–I.**

(p = 0.03). An additional analysis converting the estimated population of each cell type to the percentage of the total cell count for each case was performed to account for case-to-case variability in the total numbers of p75^{NTR}+ neurons. This correction confirmed the significant decrease in p75^{NTR}+ neurons in AD (Fig. 2D; $F_{[2, 30]}$= 3.676, p = 0.037), but also revealed a significant increase in p75^{NTR}+/TOC1+ neurons across the 3 groups examined (Fig. 2E; $F_{[2, 30]}$= 3.562, p = 0.041).

Neuropathological and Clinical Correlates

Examination of the relationship between each population of labeled CBF neurons and cognitive tests (e.g., GCS, MMSE; Table 4) revealed a significant positive correlation between the number of p75^{NTR}+ neurons and GCS (Pearson correlation r = 0.496, p = 0.003, Fig. 3A; Table 4), as well as MMSE (r = 0.53, p = 0.001; Table 4). The numbers of p75^{NTR}+/TOC1+ and TOC1+ neurons were not significantly correlated with either cognitive test (Fig. 3C, E).

The relationship between these 3 neuronal populations and neuropathological criteria (e.g., Braak stage, NIA Reagan, CERAD) is shown in Table 4. The estimated number of p75^{NTR}+ neurons correlated with all 3 measures of neuropathology. The decrease in the number of p75^{NTR}+ neurons negatively correlated with Braak stage (r = −0.43, p = 0.013; Fig. 3B; Table 4), and positively with NIA-Reagan (r = 0.52, p = 0.002) and CERAD (r = 0.51; p = 0.002) scores (Table 4). A significant positive correlation was found between the increase in the number of p75^{NTR}+/TOC1+ neurons and Braak stage (r = 0.35, p = 0.044; Fig. 3D; Table 4). No additional correlations between TOC1+ neuron number and neuropathological criteria reached statistical significance (Fig. 3F; Table 4).

Spatiotemporal Progression of TOC1+ CBF Neurons

The spatiotemporal progression of TOC1+ pathology in the CBF subfields was examined by comparing the proportion of TOC1+ neurons between the 3 clinical groups across CBF subdivisions: anterior (Ch4a; NCI, n = 10; MCI, n = 8; AD, n = 11), intermediate (Ch4i; NCI, n = 11; MCI, n = 8; AD, n = 12), and posterior (Ch4p; NCI, n = 2; MCI, n = 3; AD, n = 2) (1). The small number of cases containing Ch4p resulted from variability in tissue blocking by the brain bank at autopsy. Multiple comparison analysis revealed a significant difference between all 3 Ch4 subregions, irrespective of clinical diagnosis ($F_{[2, 84]}$=296.4, p < 0.0001; Fig. 4A). The percentage of TOC1+ nbM neurons was significantly greater in Ch4i compared to Ch4a and Ch4p, and Ch4a compared to Ch4p (Fig. 4A).

The nbM subfields contain variable numbers of cholinergic neurons, with the Ch4i subfield containing the highest density of p75^{NTR}+ neurons (1, 66). Therefore, the proportion of TOC1+ neurons relative to p75^{NTR}+ neurons within each subfield was compared to further evaluate the spread of TOC1+ pathology during the progression of AD (Fig. 4B). In NCI and MCI, the relative density of TOC1+/p75^{NTR}+ nbM neurons was highest in Ch4p compared to Ch4a and Ch4i. Conversely, the relative density of TOC1+ neurons

TABLE 3. Summary of Quantification of $p75^{NTR}$+, $p75^{NTR}$+/TOC1+, and TOC1+ Neurons

	Clinical Diagnosis			
	NCI (n = 12)	MCI (n = 9)	AD (n = 12)	Comparison by Diagnosis Group (p Value)
$p75^{NTR}$+ ($\times 10^3$)				
Mean ± SD	205.8 ± 47.6	202.1 ± 44.0	156.6 ± 57.4	0.046*
(range)	(136.8–297.9)	(148.6–277.0)	(92.6–252.0)	
$p75^{NTR}$+/TOC1+ ($\times 10^3$)				
Mean ± SD	0.9 ± 0.9	1.9 ± 2.5	6.0 ± 8.7	0.07
(range)	(0–2.4)	(0–8.4)	(0.1–31.4)	
TOC1+ ($\times 10^3$)				
Mean ± SD	0.7 ± 0.9	0.5 ± 0.5	2.3 ± 3.4	0.098
(range)	(0–2.4)	(0–1.3)	(0.07–9.6)	

AD, Alzheimer disease; MCI, mild cognitive impairment; NCI, no cognitive impairment; $p75^{NTR}$, low-affinity neurotrophin receptor; SD, standard deviation; TOC1, tau oligomer complex 1.
*Post-hoc comparison with Tukey's correction showed a significant difference between NCI and AD only.

was higher in Ch4a and Ch4i compared to Ch4p in AD, but these differences did not reach statistical significance ($p = 0.680$).

Quantification of TOC1+ Colocalization With pS422+ and MN423+

Triple-label immunofluorescence colocalization analysis of TOC1, pS422, and MN423 was used to determine the staging of tau oligomer formation during tangle maturation (56). Phosphorylation at pS422 is an early event in tangle formation, and labels prefibrillar tau pathology (12, 52, 53). Conversely, MN423 labels a tau truncation event at E391, a late event in tau evolution, indicative of mature NFT pathology (55–57, 59). Single- (TOC1+), double- (TOC1+/pS422+, TOC1+/MN423+), and triple-labeled (TOC1+/pS422+/MN423+) nbM neurons (Fig. 5) were counted in 1 section from the Ch4i subfield selected randomly from each of 6 NCI, MCI, and AD cases (Fig. 6). Quantitative analysis revealed a significant difference between the proportion of TOC1+ nbM neurons colocalizing with pS422 and/or MN423 tau pathology ($F_{[3,\ 68]}=5.006$, $p = 0.003$). Although single-labeled TOC1+ neurons were present (19.1%; Fig. 6A), TOC1 colocalized most frequently with pS422 either in the absence (33.9%) or presence (37.6%) of MN423 (Fig. 6A). Double-labeled TOC1+/MN423+ nbM neurons were observed least frequently (9.4%; Fig. 6A).

When compared between clinical groups (Fig. 6C–E), single-labeled TOC1+ neurons did not fluctuate during disease progression, remaining at ~20% (Fig. 6B). In NCI subjects, the majority of cells was double-labeled TOC1+/pS422+ (48.9%), whereas TOC1+/pS422+/MN423+ (28.6%) and TOC1+/MN423+ (3.2%) neurons were observed less frequently. The transition to MCI was marked by an increase in TOC1+/pS422+/MN423+ (49.7%) and TOC1+/MN423+ (11.4%), and a decrease in TOC1+/pS422+ (24.4%). In AD cases, the proportion of TOC1+/pS422+ (28.5%) and TOC1+/pS422+/MN423+ (34.4%) were relatively similar, whereas TOC1+/MN423+ (13.6%) increased slightly (Fig. 6C–E).

DISCUSSION

Prefibrillar forms of tau play a significant role in cognitive impairment and neurodegeneration in AD (77–79). For instance, levels of multimeric tau aggregates correlate with memory deficits in transgenic mice that overexpress tau (21). Human neurons derived from pluripotent stem cells and treated with tau oligomers, not monomers, accumulate pathologically phosphorylated tau accompanied by neurite retraction, loss of synapses, aberrant calcium homeostasis, impaired neurotransmitter signaling, and ultimately neuronal death (80). In the present study, we used unbiased stereology to evaluate the progression of tau oligomeric pathology in the Ch4 subfields, a brain region vulnerable to tau pathology and neurodegeneration early in the disease process (13, 81). We found that a decrease in the number of nbM neurons expressing the low-affinity $p75^{NTR}$ receptor, an excellent marker of CBF neurons (76), was paralleled by an increase in the number of cholinergic neurons expressing TOC1, an antibody that selectively labels oligomeric tau aggregates (24). Additionally, we demonstrate that TOC1 colocalizes extensively with pS422, an early event in tangle maturation, which spreads topographically along the caudorostral axis of the Ch4 subregions. These data indicate that formation of tau oligomers in nbM neurons follows a spatiotemporal pattern that coincides with prefibrillary tau pathology.

Loss of $p75^{NTR}$+ nbM Neurons and Increase in Tau Oligomers During AD Progression

Viability of nbM cholinergic neurons is dependent upon binding, internalization, and retrograde transport of NGF, which is mediated by a complex interaction between its 2 receptors, the high-affinity NGF-specific prosurvival tyrosine kinase TrkA and the low-affinity pan neurotrophin $p75^{NTR}$ receptor (82–4). Expression of both TrkA and $p75^{NTR}$ protein decreases within the nbM neurons in subjects with MCI and mild AD compared to NCI, suggesting a loss of neurotrophic support and cell viability (31, 76, 85). Recent work from our group suggests that accumulation of tau epitopes in nbM

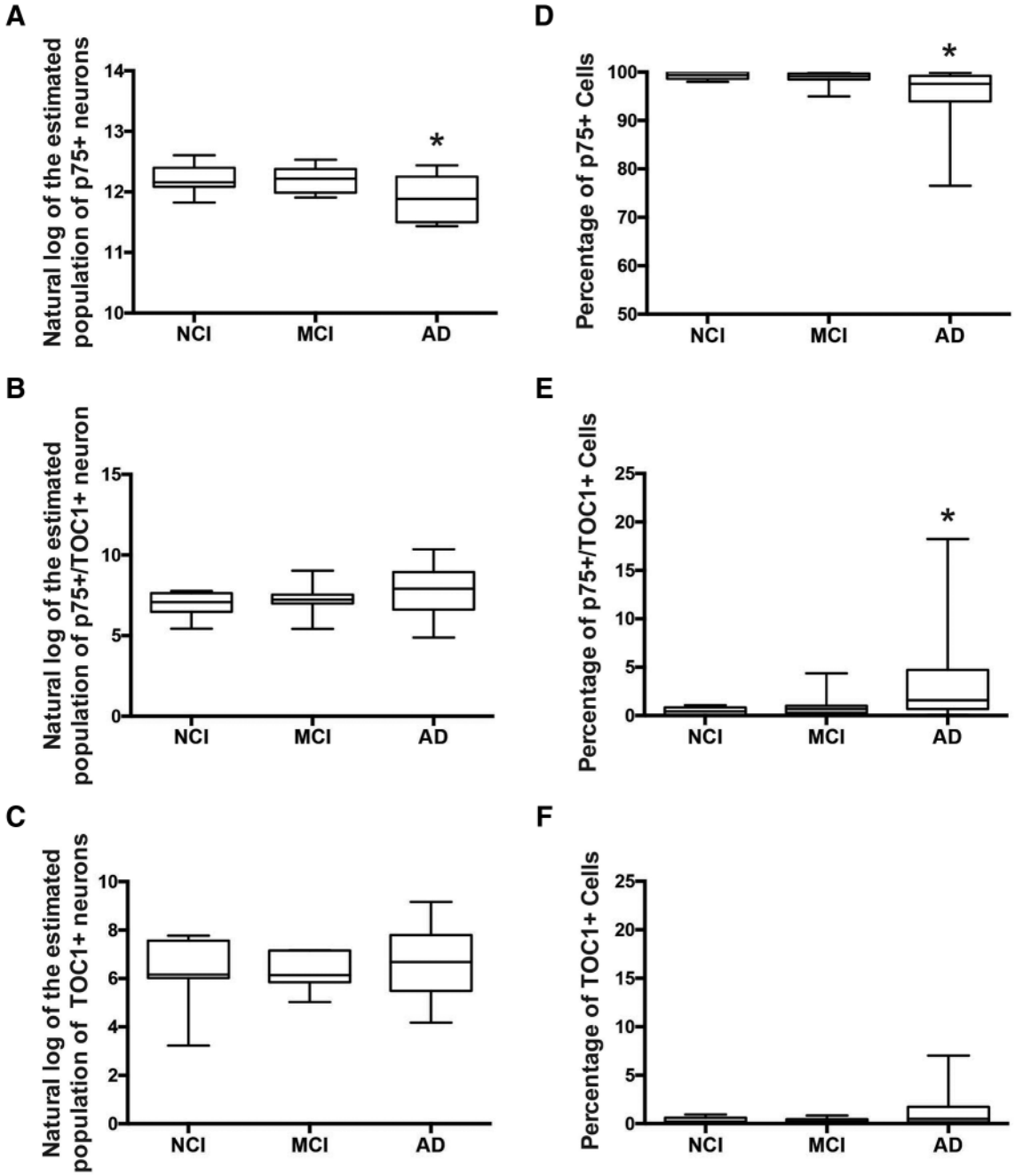

FIGURE 2. Quantification of $p75^{NTR}$+, $p75^{NTR}$+/TOC1+, and TOC1+ CBF neuron number. Box and whisker plots (max to min) of the natural log of the estimated population of $p75^{NTR}$+ **(A)**, $p75^{NTR}$+/TOC1+ **(B)**, and TOC1+ **(C)** neurons, and the percentage of $p75^{NTR}$+ **(D)**, $p75^{NTR}$+/TOC1+ **(E)**, and TOC1+ **(F)** neurons in NCI, MCI, and AD. *Significant difference compared to NCI ($p \leq 0.05$).

neurons, including pS422 and a truncation at aspartic acid-421 recognized with a TauC3 antibody, is associated with a downregulation of transcripts encoding TrkA and $p75^{NTR}$, respectively (C.T. Tiernan and S.E. Counts, unpublished data), suggesting that tau pathology underlies neuronal vulnerability across the Ch4 subfields. Furthermore, studies indicate that pS422-pseudophosphorylation enhances the formation of tau multimers and impairs axonal transport (54), implicating prefibrillar tau pathology in the dysfunction and degeneration of cholinergic nbM neurons.

In the present study, we determined whether a reduction in the number of $p75^{NTR}$+ nbM neurons was associated with increasing tau oligomer pathology labeled by the TOC1 antibody. Stereological quantification demonstrated a significant

TABLE 4. Clinical and Neuropathological Correlations with Number of $p75^{NTR}+$, $p75^{NTR}+$/TOC1+, and TOC1+ Neurons.

Age at death	$p75^{NTR}+$ NS	$p75^{NTR}+$/TOC1+ NS	TOC1+ NS
MMSE	$r = 0.53$	NS	NS
	$p = 0.001$		
Global cognitive score	$r = 0.50$	NS	NS
	$p = 0.003$		
Braak score	$r = -0.43$	$r = 0.35$	NS
	$p = 0.013$	$p = 0.044$	
Reagan diagnosis	$r = 0.52$	NS	NS
	$p = 0.002$		
CERAD diagnosis	$r = 0.51$	NS	NS
	$p = 0.002$		

MMSE, mini-mental status exam; NS, not statistically significant; $p75^{NTR}$, low-affinity neurotrophin receptor; *r*, Pearson correlation coefficient; TOC1, tau oligomer complex 1.

loss of $p75^{NTR}+$ neurons and a corresponding increase in $p75^{NTR}+$/TOC1+ and TOC1+ neurons during AD progression. Although increasing TOC1 immunoreactivity was non-significant when evaluated by estimated neuron number, the percentage of $p75^{NTR}+$ nbM neurons that were TOC1+ increased significantly by ~3.5% between NCI and AD. Moreover, $p75^{NTR}+$/TOC1+ neurons were significantly higher in NCI cases with high Braak pathology compared to those with low Braak pathology, suggesting that tau oligomer accumulation in Ch4 subfields begins in the preclinical stages of AD (86). Correlational analyses revealed a significant relationship between $p75^{NTR}+$ neurons and both cognitive (MMSE, GCS) and neuropathological (Braak score, NIA-Reagan diagnosis, and CERAD) criteria, whereas $p75^{NTR}+$/TOC1+ neurons were significantly correlated only with Braak score. A factor likely contributing to the present findings is that TOC1 immunoreactivity was apparent in only ~5% of nbM neurons, compared to ~20% of neurons containing pS422 immunoreactivity in AD (12). However, characterization of the TOC1 antibody revealed that it labels a

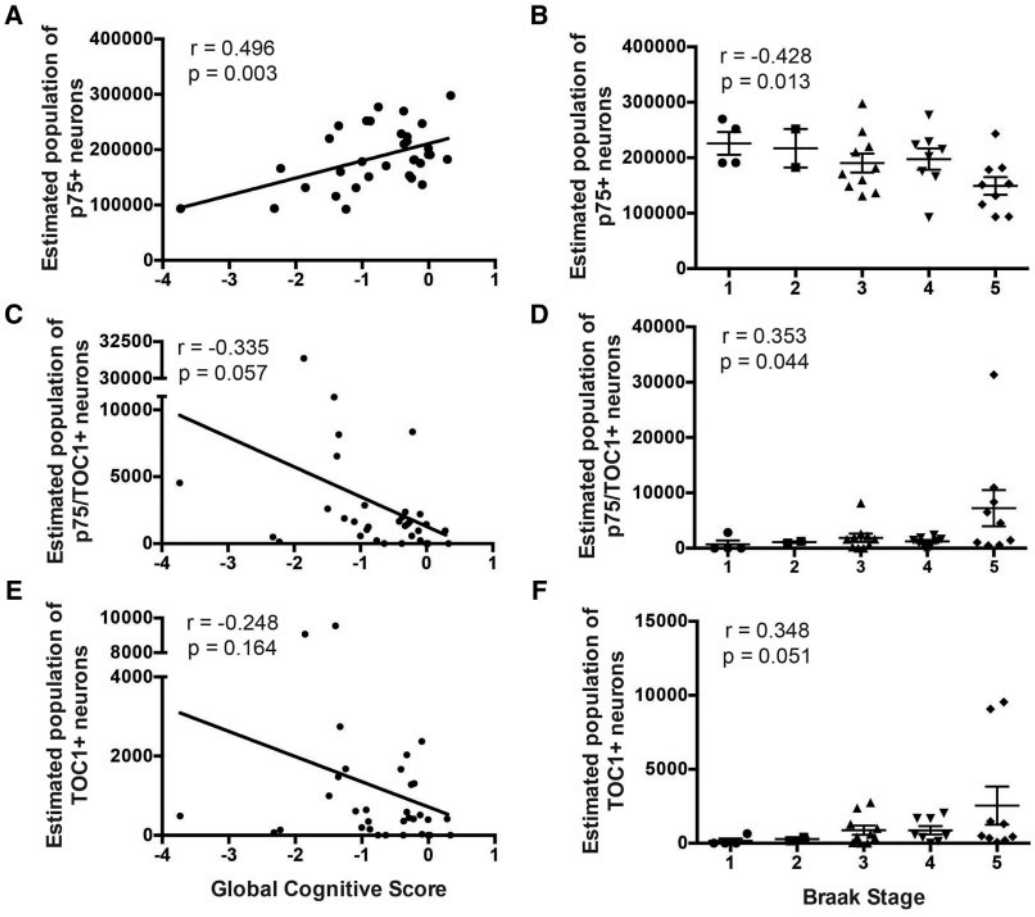

FIGURE 3. Neuropathological and clinical correlates of $p75^{NTR}+$, $p75^{NTR}+$/TOC1+, and TOC1+ nbM neuron counts. Scatterplots show a strong positive correlation between $p75^{NTR}+$ neuron number and GCS **(A)**, whereas $p75^{NTR}+$/TOC1+ **(C)** and TOC1+ **(E)** neuronal populations were not significantly correlated with GCS. Scatter dot plots (mean ± SEM) show a decrease in $p75^{NTR}+$ neurons **(B)** compared with an increase in $p75^{NTR}+$/TOC1+ **(D)** and TOC1+ **(F)** neurons across Braak stages. Braak stage was significantly correlated with the decrease in $p75^{NTR}+$ neurons, and the increase in $p75^{NTR}+$/TOC1+ neurons. *r* = Pearson correlation.

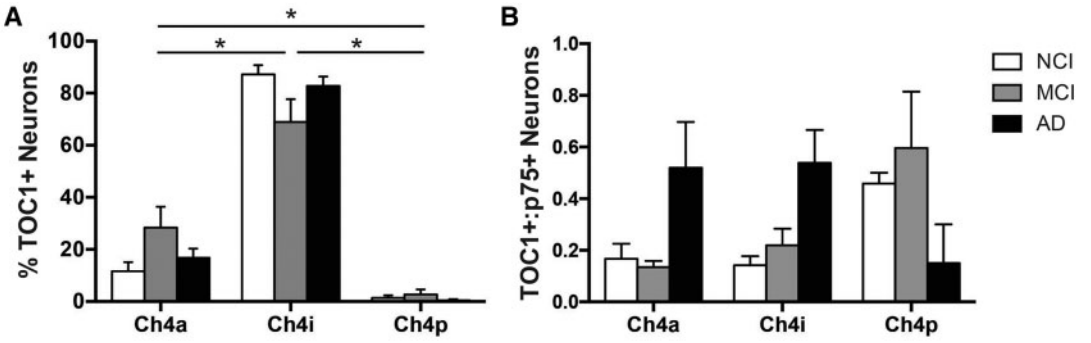

FIGURE 4. Ch4 subregional spatiotemporal progression of TOC1+ pathology. Histograms (mean ± SEM) of the percentage of TOC1+ neurons (including both $p75^{NTR}$+/TOC1+ and TOC1+ neurons); **(A)** and the ratio of TOC1+ neurons to $p75^{NTR}$+ neurons **(B)** in each subdivision (anterior, intermediate, posterior) of the CBF by clinical group (NCI, white bars; MCI, gray bars; AD, black bars). *Significant difference between groups ($p < 0.05$).

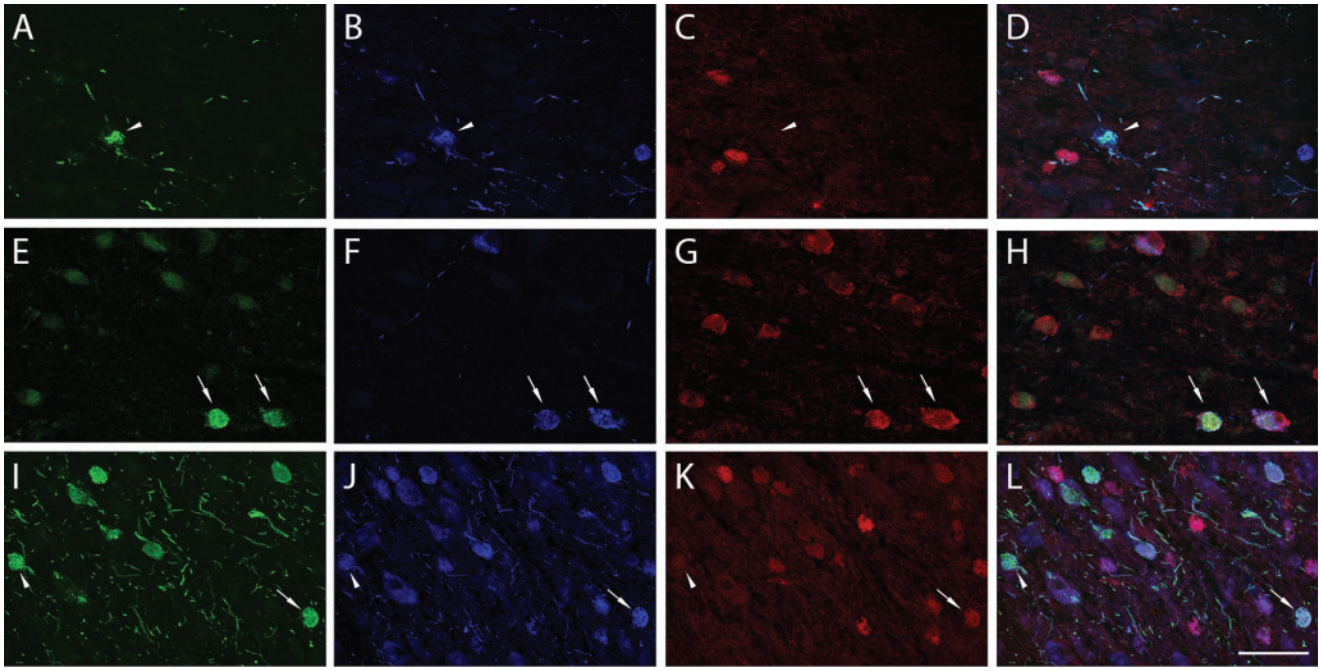

FIGURE 5. Triple immunofluorescence of TOC1, pS422, and MN423. Immunofluorescence of TOC1 (green), pS422 (blue), and MN423 (red) in the nbM revealed a relatively higher proportion of TOC1+/pS422+ neurons (arrowhead) in NCI (**A–D)** and MCI **(E–H)** cases. In MCI, MN423 staining was observed more frequently and thus the number of TOC1+/pS422+/MN423+ neurons (arrow) increased. Triple-labeled NB neurons were also observed in AD (**H–L**; arrow), however, double-labeled TOC1+/pS422+ neurons persisted in AD (arrowhead). Scale bar: **L** = 100 μm, and applies to all images.

subpopulation of tau oligomers (24). Thus, it is reasonable to speculate that additional, as yet undefined oligomeric tau conformations also accumulate within Ch4 neurons during the progression of AD. The mechanism by which tau oligomers contribute to cholinergic nbM neuronal dysfunction and degeneration is not well established. However, evidence suggests that prefibrillar species of tau contribute to neuronal pathology through a diverse range of cellular processes, including impairment of long-term potentiation and memory consolidation (21, 27, 87), inhibition of axonal transport (88), and mitochondrial and synaptic dysfunction (22, 87).

Tau Oligomer Formation During NFT Maturation

In AD, the evolution of NFT formation appears to follow a relatively ordered series of events (56). This process involves aberrant phosphorylation, conformational changes, and truncation of the termini of tau proteins within these inclusions (53, 56, 57, 89). Presently, we used triple-label confocal microscopy to investigate the contribution of tau oligomer formation to the formation of NFTs in nbM neurons by examining TOC1+ colocalization with the pretangle marker pS422 (52, 53, 90, 91) and MN423, a tau epitope that is associated

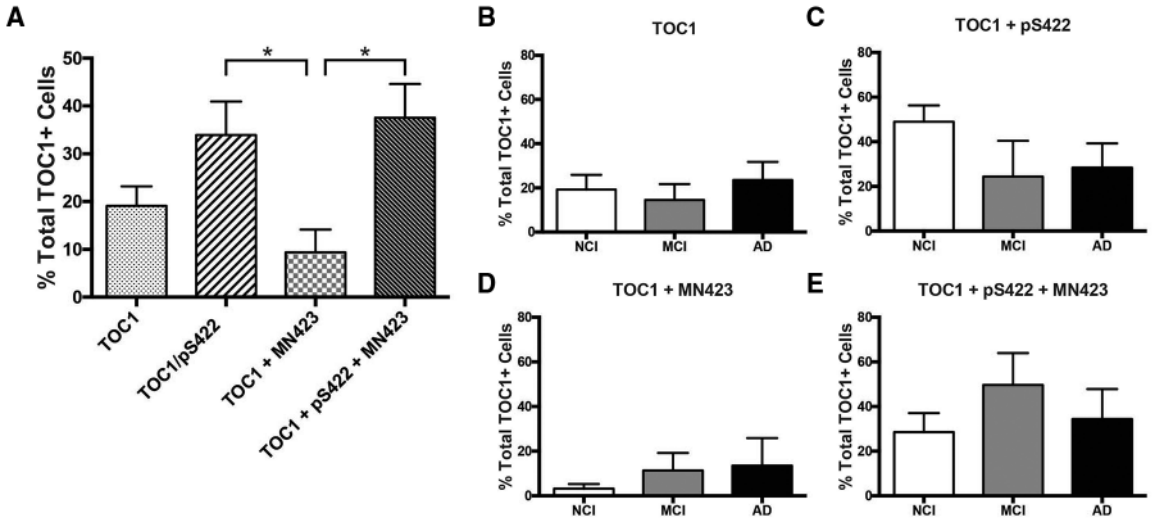

FIGURE 6. Quantification of TOC1+, TOC1+/pS422+, TOC1+/MN423+, and TOC1+/pS422+/MN423+ nbM neuron number. Histograms (mean ± SEM) of percentage of TOC1+ neurons single-, double-, or triple-labeled in all cases **(A)** or by clinical group **(B–E)**. *Significant difference between groups ($p \leq 0.05$).

with mature NFT pathology (55, 57–59). Approximately 72% of all TOC1+ nbM neurons also contained pS422+, either in the absence (34%) or in the presence (38%) of MN423. Double-labeled TOC1+/MN423+ nbM neurons were rare (9%). These data suggest that tau oligomer formation in Ch4 perikarya is an early event in tangle maturation, consistent with previous reports (24, 54, 92, 93). When compared across clinical groups, we observed a temporal shift in the distribution of the colocalization of these markers. In NCI, TOC1 primarily colocalized with pS422. The transition to MCI and AD was marked by an increased presence of TOC1+/MN423+ pathology, indicative of tangle maturation, and a shift away from double-labeled TOC1+/pS422+ toward triple-labeled TOC1+/pS422+/MN423+ positive neurons, accordingly. Taken together, these findings imply a specific order of epitope occurrence in the cholinergic neurons of the nbM that progresses from pS422 → TOC1 → MN423. In this scheme, aberrant phosphorylation, including pS422, primes the tau protein for additional phosphorylation events and conformational changes (89, 94) that facilitate oligomerization (95). Once aggregation is initiated, truncation events such as cleavage at E391 ensue (56).

nbM Subfield Spatiotemporal Pattern of Tau Oligomers

Cholinergic neurons within the nbM are classically subdivided into anterior (Ch4a; in many cases further subdivided into anteromedial and anterolateral), intermediate (Ch4i), and posterior (Ch4p) cell groups (1, 2, 10, 16, 66). One of the primary goals of this study was to characterize the regional distribution of tau pathology in Ch4 subfields as this chemospecific cell population is selectively vulnerable during the progression of AD (6, 8–10, 14, 15, 96–100). However, few studies have investigated Ch4 regional susceptibility to neuronal pathology (9, 10, 14–16, 98, 99), and to our knowledge, none has investigated the topographic pattern of oligomeric, phosphorylated or truncated tau pathology within this region. The majority of studies characterizing nbM neuronal cell loss have reported a caudorostral pattern during AD progression, with Ch4p being most severely affected (9, 10, 14–16). However, a minority of studies have reported the greatest decline in Ch4a (98, 99). The present study provides evidence that tau oligomer pathology follows a caudorostral gradient supporting a Ch4p → Ch4a pattern of neuronal vulnerability. When normalized to regional cell number, TOC1+ labeling was greatest in Ch4p during the progression from NCI to MCI, and in Ch4a and Ch4i once clinical AD was manifest. Given the evidence that prefibrillar tau pathology is associated with molecular and cellular abnormalities within nbM neurons (11), appearance of prefibrillar oligomeric tau likely precedes cell loss. On the basis of the current findings, TOC1 pathology would be greater in Ch4p during the NCI and MCI stages, as observed. Conversely, frank cell death in Ch4p during later disease stages (i.e., mild/moderate AD) would shift the burden of TOC1 pathology to more rostral subdivisions (i.e., Ch4a, Ch4i). As only a subset of cases used here included Ch4p, analysis of a larger sample containing the posterior subfield should be undertaken. In this regard, we encourage both national and international brain banks to collect the entire CBF for future clinical pathological investigations.

Interestingly, the caudal to rostral pattern of Ch4 tau pathology may underlie the pathobiology associated with its topographical cortical innervation. Combined retrograde cell tracer and acetylcholinesterase histochemical studies demonstrated that Ch4a projects to medial cortical regions, Ch4i to laterodorsal frontoparietal areas, and Ch4p to the temporal cortex in the macaque monkey (1). Here, we found the greatest load of tau oligomer neuronal immunoreactivity in Ch4p, which also displays the highest level of CBF neuronal loss (9, 10, 14–16). These observations in Ch4p are intriguing in light of recent imaging studies showing that Ch4 volume loss is

associated with notable reductions in temporal cortical thickness, as well as cognitive decline, in MCI and AD (101–103).

In summary, these results identify a spatiotemporal pattern of tau oligomer pathology in the Ch4 subfields of the nbM during the progression of AD. Oligomeric tau, identified by the TOC1 antibody, appeared concomitant with a decrease in $p75^{NTR}$ nbM neurons during the transition from MCI to AD. Furthermore, the formation of tau oligomers in Ch4 occurs relatively early in the process of tangle maturation, which proceeds along a caudorostral gradient during the progression from NCI to MCI to AD. Future work is needed to determine whether other markers of tau pathology follow a similar topographical pattern during disease progression. Even so, the present findings provide important and novel evidence for a regional pattern of tau pathology within the cholinergic neurons of the nbM that contributes to neuronal loss and cognitive decline in AD.

ACKNOWLEDGMENT

We are indebted to the altruism and support of the Rush Religious Order Study participants.

REFERENCES

1. Mesulam M, Mufson EJ, Levey AI, et al. Cholinergic innervation of cortex by the basal forebrain: cytochemistry and cortical connections of the septal area, diagonal band nuclei, nucleus basalis (substantia innominata), and hypothalamus in the rhesus monkey. J Comp Neurol 1983; 214:170–97
2. Mesulam MM, Geula C. Nucleus basalis (Ch4) and cortical cholinergic innervation in the human brain: Observations based on the distribution of acetylcholinesterase and choline acetyltransferase. J Comp Neurol 1988;275:216–40
3. Bierer LM, Haroutunian V, Gabriel S, et al. Neurochemical correlates of dementia severity in Alzheimer's disease: Relative importance of the cholinergic deficits. J Neurochem 1995;64:749–60
4. Pappas BA, Bayley PJ, Bui BK, et al. Choline acetyltransferase activity and cognitive domain scores of Alzheimer's patients. Neurobiol Aging 2000;21:11–7
5. Wilcock GK, Esiri MM. Plaques, tangles and dementia. A quantitative study. J Neurol Sci 1982;56:343–56
6. Whitehouse PJ, Price DL, Struble RG, et al. Alzheimers-disease and senile dementia—Loss of neurons in the basal forebrain. Science 1982; 215:1237–9
7. McGeer PL, McGeer EG, Suzuki J, et al. Aging, Alzheimer's disease, and the cholinergic system of the basal forebrain. Neurol Sci 1984;34: 741–5.
8. Tagliavini F, Pilleri G. Neuronal counts in basal nucleus of Meynert in Alzheimer disease and in simple senile dementia. Lancet 1983;1: 469–70
9. Arendt T, Bigl V, Tennstedt A, et al. Neuronal loss in different parts of the nucleus basalis is related to neuritic plaque formation in cortical target areas in Alzheimer's disease. Neuroscience 1985;14:1–14
10. Mufson EJ, Bothwell M, Kordower JH. Loss of nerve growth-factor receptor-containing neurons in Alzheimers-disease—A quantitative-analysis across subregions of the basal forebrain. Exp Neurol 1989;105: 221–32
11. Tiernan CT, Ginsberg SD, Guillozet-Bongaarts AL, et al. Neurobiology of aging. Neurobiol Aging 2016;42:80–90
12. Vana L, Kanaan NM, Ugwu IC, et al. Progression of tau pathology in cholinergic basal forebrain neurons in mild cognitive impairment and Alzheimer's disease. Am J Pathol 2011;179:2533–50
13. Mesulam M, Shaw P, Mash D, et al. Cholinergic nucleus basalis tauopathy emerges early in the aging-MCI-AD continuum. Ann Neurol 2004; 55:815–28
14. Wilcock GK, Esiri MM, Bowen DM, et al. The differential involvement of subcortical nuclei in senile dementia of Alzheimer's type. J Neurol Neurosurg Psychiatry 1988;51:842–9
15. Iraizoz I, Guijarro JL, Gonzalo LM, et al. Neuropathological changes in the nucleus basalis correlate with clinical measures of dementia. Acta Neuropathol 1999;98:186–96
16. Liu AKL, Chang RC-C, Pearce RKB, et al. Nucleus basalis of Meynert revisited: Anatomy, history and differential involvement in Alzheimer's and Parkinson's disease. Acta Neuropathol 2015;129:527–40
17. Arriagada PV, Growdon JH, Hedley-Whyte ET, et al. Neurofibrillary tangles but not senile plaques parallel duration and severity of Alzheimer's disease. Neurol Sci 1992;42:631–9
18. Gómez-Isla T, Hollister R, West H, et al. Neuronal loss correlates with but exceeds neurofibrillary tangles in Alzheimer's disease. Ann Neurol 1997;41:17–24
19. Gotz J, Chen F, Van Dorpe J, et al. Formation of neurofibrillary tangles in P301L tau transgenic mice induced by A beta 42 fibrils. Science 2001;293:1491–5
20. Bennett DA, Schneider JA, Wilson RS, et al. Neurofibrillary tangles mediate the association of amyloid load with clinical Alzheimer disease and level of cognitive function. Arch Neurol 2004;61:378–84
21. Berger Z, Roder H, Hanna A, et al. Accumulation of pathological tau species and memory loss in a conditional model of tauopathy. J Neurosci 2007;27:3650–62
22. Kopeikina KJ, Carlson GA, Pitstick R, et al. Tau accumulation causes mitochondrial distribution deficits in neurons in a mouse model of tauopathy and in human Alzheimer's disease brain. Am J Pathol 2011;179: 2071–82
23. Maeda S, Sahara N, Saito Y, et al. Granular tau oligomers as intermediates of tau filaments. Biochemistry 2007;46:3856–61
24. Patterson KR, Remmers C, Fu Y, et al. Characterization of prefibrillar tau oligomers in vitro and in Alzheimer disease. J Biol Chem 2011;286: 23063–76
25. Sahara N, DeTure M, Ren Y, et al. Characteristics of TBS-extractable hyperphosphorylated tau species: Aggregation intermediates in rTg4510 mouse brain. J Alzheimers Dis 2013;33:249–63
26. Santacruz K, Lewis J, Spires T, et al. Tau suppression in a neurodegenerative mouse model improves memory function. Science 2005;309: 476–81
27. Fá M, Puzzo D, Piacentini R, et al. Extracellular tau oligomers produce an immediate impairment of LTP and memory. Sci Rep 2016;6:1–15
28. Maeda S, Sahara N, Saito Y, et al. Increased levels of granular tau oligomers: An early sign of brain aging and Alzheimer's disease. Neurosci Res 2006;54:197–201
29. Braak H, Braak E. Frequency of stages of Alzheimer-related lesions in different age categories. Neurobiol Aging 1997;18:351–7
30. Mufson EJ, Chen EY, Cochran EJ, et al. Entorhinal cortex β-amyloid load in individuals with mild cognitive impairment. Exp Neurol 1999; 158:469–90
31. Mufson EJ, Ma SY, Cochran EJ, et al. Loss of nucleus basalis neurons containing trkA immunoreactivity in individuals with mild cognitive impairment and early Alzheimer's disease. J Comp Neurol 2000;427: 19–30
32. Kordower JH, Chu Y, Stebbins GT, et al. Loss and atrophy of layer II entorhinal cortex neurons in elderly people with mild cognitive impairment. Ann Neurol 2001;49:202–13
33. Gilmor ML, Erickson JD, Varoqui H, et al. Preservation of nucleus basalis neurons containing choline acetyltransferase and the vesicular acetylcholine transporter in the elderly with mild cognitive impairment and early Alzheimer's disease. J Comp Neurol 1999;411:693–704
34. Bennett DA, Shannon KM, Beckett LA, et al. Dimensionality of parkinsonian signs in aging and Alzheimer's disease. J Gerontol A Biol Sci Med Sci 1999;54:M191–6
35. Bennett DA, Shannon KM, Beckett LA, et al. Metric properties of nurses' ratings of parkinsonian signs with a modified Unified Parkinson's Disease Rating Scale. Neurol Sci 1997;49:1580–7
36. Counts SE, Nadeem M, Wuu J, et al. Reduction of cortical TrkA but not p75NTR protein in early-stage Alzheimer's disease. Ann Neurol 2004; 56:520–31
37. Pittman J, Andrews H, Tatemichi T, et al. Diagnosis of dementia in a heterogeneous population: A comparison of paradigm-based diagnosis and physician's diagnosis. Arch Neurol 1992;49:461–7

38. Snowdon DA, Kemper SJ, Mortimer JA, et al. Linguistic ability in early life and cognitive function and Alzheimer's disease in late life. Findings from the Nun Study. JAMA 1996;275:528–32
39. Chen C, Li X, Wang T, et al. Association between NMDA receptor subunit 2b gene polymorphism and Alzheimer's disease in Chienes Han population in Shanghai. Neurol Sci 1984;34:939–44
40. Devanand DP, Folz M, Gorlyn M, et al. Questionable dementia: Clinical course and predictors of outcome. J Am Geriatr Soc 1997;45:321–8
41. Petersen RC, Smith GE, Ivnik RJ, et al. Apolipoprotein E status as a predictor of the development of Alzheimer's disease in memory-impaired individuals. JAMA 1995;273:1274–8
42. Flicker C, Ferris SH, Reisberg B. Mild cognitive impairment in the elderly: Predictors of dementia. Neurol Sci 1991;41:1006–9
43. Rubin EH, Morris JC, Grant EA, et al. Very mild senile dementia of the Alzheimer type. I. Clinical assessment. Arch Neurol 1989;46:379–82
44. Cochran EJ, Fox JH, Mufson EJ. Severe panencephalic Pick's disease with Alzheimer's disease-like neuropil threads and synaptophysin immunoreactivity. Acta Neuropathol 1994;88:479–84
45. Mirra SS, Heyman A, McKeel D, et al. The Consortium to Establish a Registry for Alzheimer's Disease (CERAD) Part II. Standardization of the neuropathologic assessment of Alzheimer's disease. Neurol Sci 1991;41:479–86
46. Braak H, Braak E. Neuropathological staging of Alzheimer-related changes. Acta Neuropathol 1991;82:239–59
47. Hyman BT, Trojanowski JQ. Consensus recommendations for the postmortem diagnosis of Alzheimer disease from the National Institute on Aging and the Reagan Institute Working Group on diagnostic criteria for the neuropathological assessment of Alzheimer disease. J Neuropathol Exp Neurol 1997;56:1095–7
48. Dubois B, Feldman HH, Jacova C, et al. Research criteria for the diagnosis of Alzheimer's disease: Revising the NINCDS-ADRDA criteria. Lancet Neurol 2007;6:734–46
49. Ward SM, Himmelstein DS, Lancia JK, et al. TOC1: Characterization of a selective oligomeric tau antibody. J Alzheimers Dis 2013;37: 593–602
50. Kordower JH, Bartus RT, Bothwell M, et al. Nerve growth factor receptor immunoreactivity in the nonhuman primate (*Cebus apella*): Distribution, morphology, and colocalization with cholinergic enzymes. J Comp Neurol 1988;277:465–86
51. Schatteman GC, Gibbs L, Lanahan AA, et al. Expression of NGF receptor in the developing and adult primate central nervous system. J Neurosci 1988;8:860–73
52. Guillozet-Bongaarts AL, Cahill ME, Cryns VL, et al. Pseudophosphorylation of tau at serine 422 inhibits caspase cleavage: In vitro evidence and implications for tangle formation in vivo. J Neurochem 2006;97: 1005–14
53. Kimura T, Ono T, Takamatsu J, et al. Sequential changes of tau-site-specific phosphorylation during development of paired helical filaments. Dementia 1996;7:177–81
54. Tiernan CT, Combs B, Cox K, et al. Pseudophosphorylation of tau at S422 enhances SDS-stable dimer formation and impairs both anterograde and retrograde fast axonal transport. Exp Neurol 2016;283: 318–29
55. García-Sierra F, Ghoshal N, Quinn B, et al. Conformational changes and truncation of tau protein during tangle evolution in Alzheimer's disease. JAD 2003;5:65–77
56. Binder LI, Guillozet-Bongaarts AL, García-Sierra F, et al. Tau, tangles, and Alzheimer's disease. Biochim Biophys Acta 2005;1739:216–23
57. Guillozet-Bongaarts AL, García-Sierra F, Reynolds MR, et al. Tau truncation during neurofibrillary tangle evolution in Alzheimer's disease. Neurobiol Aging 2005;26:1015–22
58. Harrington CR, Mukaetova-Ladinska EB, Hills R, et al. Measurement of distinct immunochemical presentations of tau protein in Alzheimer disease. Proc Natl Acad Sci U S A 1991;88:5842–6
59. Novak M, Wischik CM, Edwards P, et al. Characterisation of the first monoclonal antibody against the pronase resistant core of the Alzheimer PHF. Prog Clin Biol Res 1989;317:755–61
60. Kanaan NM, Kordower JH, Collier TJ. Age-related accumulation of Marinesco bodies and lipofuscin in rhesus monkey midbrain dopamine neurons: Relevance to selective neuronal vulnerability. J Comp Neurol 2007;502:683–700
61. Kanaan NM, Morfini GA, LaPointe NE, et al. Pathogenic forms of tau inhibit kinesin-dependent axonal transport through a mechanism involving activation of axonal phosphotransferases. J Neurosci 2011;31: 9858–68
62. Kanaan NM, Morfini G, Pigino G, et al. Phosphorylation in the amino terminus of tau prevents inhibition of anterograde axonal transport. Neurobiol Aging 2012;33:826.e15–.e30
63. Mufson EJ, Counts SE, Ginsberg SD. Gene expression profiles of cholinergic nucleus basalis neurons in Alzheimer's disease. Neurochem Res 2002;27:1035–48
64. Gundersen HJ, Bagger P, Bendtsen TF, et al. The new stereological tools: Disector, fractionator, nucleator and point sampled intercepts and their use in pathological research and diagnosis. APMIS 1988;96: 857–81
65. Pakkenberg B, Møller A, Gundersen HJ, et al. The absolute number of nerve cells in substantia nigra in normal subjects and in patients with Parkinson's disease estimated with an unbiased stereological method. J Neurol Sci 1991;54:30–3
66. Halliday GM, Cullen K, Cairns MJ. Quantitation and three-dimensional reconstruction of Ch4 nucleus in the human basal forebrain. Synapse 1993;15:1–16
67. West MJ. New stereological methods for counting neurons. Neurobiol Aging 1993;14:275–85
68. West MJ. Stereological methods for estimating the total number of neurons and synapses: Issues of precision and bias. Trends Neurosci 1999; 22:51–61
69. Gundersen HJ, Jensen EB, Kiêu K, et al. The efficiency of systematic sampling in stereology–reconsidered. J Microsc 1999;193:199–211
70. West MJ, Gundersen HJ. Unbiased stereological estimation of the number of neurons in the human hippocampus. J Comp Neurol 1990;296: 1–22
71. Kelly SC, Bin H, Perez SE, et al. Locus coeruleus cellular and molecular pathology during the progression of Alzheimer's disease. Acta Neuropathol Commun 2017;5:8
72. Counts SE, Nadeem M, Lad SP, et al. Differential expression of synaptic proteins in the frontal and temporal cortex of elderly subjects with mild cognitive impairment. J Neuropathol Exp Neurol 2006;65: 592–601
73. Price JL, McKeel DW, Jr., Buckles VD, et al. Neuropathology of nondemented aging: Presumptive evidence for preclinical Alzheimer disease. Neurobiol Aging 2009;30:1026–36
74. Markesbery WR. Neuropathologic alterations in mild cognitive impairment: A review. J Alzheimers Dis 2010;19:221–8
75. Mufson EJ, Malek-Ahmadi M, Snyder N, et al. Neurobiol Aging 2016; 43:101–10
76. Mufson EJ, Ma SY, Dills J, et al. Loss of basal forebrain P75NTR immunoreactivity in subjects with mild cognitive impairment and Alzheimer's disease. J Comp Neurol 2002;443:136–53
77. Brunden KR, Trojanowski JQ, Lee VM-Y. Evidence that non-fibrillar tau causes pathology linked to neurodegeneration and behavioral impairments. J Alzheimers Dis 2008;14:393–9
78. Ward SM, Himmelstein DS, Lancia JK, et al. Tau oligomers and tau toxicity in neurodegenerative disease. Biochem Soc Trans 2012;40: 667–71
79. Cárdenas-Aguayo MADC, Gómez-Virgilio L, DeRosa S, et al. The role of tau oligomers in the onset of Alzheimer's disease neuropathology. ACS Chem Neurosci 2014;5:1178–91
80. Usenovic M, Niroomand S, Drolet RE, et al. Internalized tau oligomers cause neurodegeneration by inducing accumulation of pathogenic tau in human neurons derived from induced pluripotent stem cells. J Neurosci 2015;35:14234–50
81. Sassin I, Schultz C, Thal DR, et al. Evolution of Alzheimer's disease-related cytoskeletal changes in the basal nucleus of Meynert. Acta Neuropathol 2000;100:259–69
82. Kaplan DR, Miller FD. Neurotrophin signal transduction in the nervous system. Curr Opin Neurobiol 2000;10:381–91
83. Sofroniew MV, Howe CL, Mobley WC. Nerve growth factor signaling, neuroprotection, and neural repair. Annu Rev Neurosci 2001;24: 1217–81
84. Teng KK, Hempstead BL. Neurotrophins and their receptors: Signaling trios in complex biological systems. Cell Mol Life Sci 2004;61:35–48

85. Mufson EJ, Lavine N, Kordower JH, et al. Reduction in p140-TrkA receptor protein within the nucleus basalis and cortex in Alzheimer's disease. Exp Neurol 1997;146:91–103
86. Jicha GA, Abner EL, Schmitt FA, et al. Preclinical AD Workgroup staging: Pathological correlates and potential challenges. Neurobiol Aging 2012;33:622.e1–.e16
87. Lasagna-Reeves CA, Castillo-Carranza DL, Sengupta U, et al. Tau oligomers impair memory and induce synaptic and mitochondrial dysfunction in wild-type mice. Mol Neurodegeneration 2011;6:39
88. Patterson KR, Ward SM, Combs B, et al. Heat shock protein 70 prevents both tau aggregation and the inhibitory effects of preexisting tau aggregates on fast axonal transport. Biochemistry 2011;50:10300–10
89. Bertrand J, Plouffe V, Sénéchal P, et al. The pattern of human tau phosphorylation is the result of priming and feedback events in primary hippocampal neurons. Neuroscience 2010;168:323–34
90. Hasegawa M, Jakes R, Crowther RA, et al. Characterization of mAb AP422, a novel phosphorylation-dependent monoclonal antibody against tau protein. FEBS Lett 1996;384:25–30
91. Bussière T, Hof PR, Mailliot C, et al. Phosphorylated serine422 on tau proteins is a pathological epitope found in several diseases with neurofibrillary degeneration. Acta Neuropathol 1999;97:221–30
92. Mufson EJ, Ward S, Binder L. Prefibrillar tau oligomers in mild cognitive impairment and Alzheimer's disease. Neurodegener Dis 2014;13:151–3
93. Lasagna-Reeves CA, Castillo-Carranza DL, Sengupta U, et al. Identification of oligomers at early stages of tau aggregation in Alzheimer's disease. FASEB J 2012;26:1946–59
94. Luna-Munoz J, Chavez-Macias L, Garcia-Sierra F, et al. Earliest stages of tau conformational changes are related to the appearance of a sequence of specific phospho-dependent tau epitopes in Alzheimer's disease. J Alzheimers Dis 2007;12:365–75
95. Iqbal K. Hyperphosphorylation-induced tau oligomers. Front Neurol 2013;4:1–9
96. Whitehouse PJ, Price DL, Clark AW, et al. Alzheimer-disease—Evidence for selective loss of cholinergic neurons in the nucleus basalis. Ann Neurol 1981;10:122–6
97. Candy JM, Perry RH, Perry EK, et al. Pathological-changes in the nucleus of Meynert in Alzheimers and Parkinsons diseases. J Neurol Sci 1983;59:277–89
98. Doucette R, Fisman M, Hachinski VC, et al. Cell loss from the nucleus basalis of Meynert in Alzheimer's disease. Can J Neurol Sci 1986;13:435–40
99. Iraizoz I, de Lacalle S, Gonzalo LM. Cell loss and nuclear hypertrophy in topographical subdivisions of the nucleus basalis of Meynert in Alzheimer's disease. Neuroscience 1991;41:33–40
100. Wilcock GK, Esiri MM, Bowen DM, et al. The nucleus basalis in Alzheimer's disease: Cell counts and cortical biochemistry. Neuropathol Appl Neurobiol 1983;9:175–9
101. Cantero JL, Zaborszky L, Atienza M. Volume loss of the nucleus basalis of Meynert is associated with atrophy of innervated regions in mild cognitive impairment. Cereb Cortex 2017;27:3881–9
102. Grothe M, Zaborszky L, Atienza M, et al. Reduction of basal forebrain cholinergic system parallels cognitive impairment in patients at high risk of developing Alzheimer's disease. Cereb Cortex 2010;20:1685–95
103. Grothe MJ, Heinsen H, Amaro EJ, et al. Cognitive correlates of basal forebrain atrophy and associated cortical hypometabolism in mild cognitive impairment. Cereb Cortex 2016;26:2411–26